Materials Science & Engineering A 852 (2022) 143680

Contents lists available at ScienceDirect

Materials Science & Engineering A

journal homepage: www.elsevier.com/locate/msea

Compression behaviour of TPMS-filled stainless steel tubes

Nejc Novak [a,*], Dan Kytyr [b], Vaclav Rada [b,c], Tomas Doktor [c], Oraib Al-Ketan [d], Reza Rowshan [d], Matej Vesenjak [a], Zoran Ren [a]

[a] Faculty of Mechanical Engineering, University of Maribor, Maribor, Slovenia
[b] Czech Academy of Sciences, Institute of Theoretical and Applied Mechanics, Prague, Czech Republic
[c] Czech Technical University in Prague, Faculty of Transportation Sciences, Prague, Czech Republic
[d] Core Technology Platforms Operations, New York University Abu Dhabi, Abu Dhabi, United Arab Emirates

ARTICLE INFO

Keywords:
Cellular structure
Triply periodical minimal surface
TPMS
TPMS-filled tube
Compressive loading
Experimental testing
Computational modelling
Homogenised core

ABSTRACT

One of the most promising options for future crashworthiness applications is thin-walled tubes filled with various cellular materials (e.g. metal foam). Of higher interest are the shell-based lattices, which have lately gained popularity due to their superior qualities over strut-based lattices. In this work, we investigate the mechanical response of foam-filled tubes where the tube's core was represented by Triply Periodic Minimal Surface (TPMS) diamond lattices. Samples made of stainless steel 316L comprising the diamond lattice core, empty tubes, and in-situ TPMS-filled tubes were additively manufactured and mechanically tested under compressive loading. As-fabricated welded tubes and ex-situ TPMS-filled tubes were also analysed and compared. Under the axial loading, the ex-situ and in-situ TPMS-filled tubes showed very similar behaviour. Enhanced energy absorption up to 21% and 44% compared to the sum of empty tubes and the core responses was noted. The energy absorption enhancement of 12% in the case of transversal loading is limited to in-situ TPMS-filled tubes, where the connection between the tube and core prevents the tube's walls from buckling. Computational models with homogenised core were developed and validated based on the experimental data. These straightforward, fast, and accurate computational models can be efficiently used for large-scale real-life applications, e.g. crash and impact.

1. Introduction

In the case of impact or crash, the energy-absorbing component transforms the impact energy created during a collision event to provide the best possible protection for passengers, vehicles, and buildings [1]. Due to the crashworthiness performance, low prices, and consistent manufacture, the thin-walled tubes are extensively used as an impact energy-absorbing component in numerous industry domains. Even while a thin-walled straight tube has clear benefits in terms of energy absorption, it has a high peak collapse load followed by an abrupt load decrease when dispersing impact energy. This can be limited to using tapered tubes, which attracted the attention of many researchers [2,3]. The deformation behaviour and energy absorption of straight and frusta tubes with different profiles were studied in Ref. [4]. The research stated that the tube's energy absorption is influenced by its cross-section and that the peak collapsing load of the frusta tube is smaller than that of the corresponding straight tube. Besides tapering, also foam-filled tubes can contribute to more uniform stress distribution and higher energy absorption capabilities.

Foams and other cellular (meta)materials are made of an interconnected network of solid struts or sheets which form the cell's edges and faces. Their mechanical behaviour depends mainly on the relative density (porosity) and the base material, which can be metal or non-metal [5–7]. With careful choice of the above parameters and proper fabrication procedure of a cellular metamaterial, it is possible to achieve their various mechanical (strength, stiffness) and thermal properties (thermal conductivity). The advantages of cellular structures and cellular metamaterials, in general, are low density (lightweight structures), efficient damping, high rate of deformation, high energy absorption capability, durability at dynamic loadings and fatigue, high thermal and acoustic isolation [7]. Their mechanical and thermal properties make them very suitable for use in automotive, railway, naval, marine, aerospace industry, and medicine, as well as in general lightweight machine design as filters, heat exchangers, isolators,

* Corresponding author.
E-mail address: n.novak@um.si (N. Novak).

https://doi.org/10.1016/j.msea.2022.143680
Received 3 March 2022; Received in revised form 19 July 2022; Accepted 21 July 2022
Available online 1 August 2022
0921-5093/© 2022 The Authors. Published by Elsevier B.V. This is an open access article under the CC BY-NC-ND license (http://creativecommons.org/licenses/by-nc-nd/4.0/).

bearings, core material in sandwich structures and as fillers in hollow parts for additional stiffness/support, impact energy absorption and damping [8]. For example, Hanssen et al. [9] investigated the behaviour of the foam-filled square tube made from aluminium and filled with aluminium closed-cell foam. There are many studies regarding the axial compression loading of foam-filled tubes available in the literature. The ex-situ [10] and in-situ [11] aluminium foam-filled tubes showed improved crush performance under axial compressive loads compared to empty tubes. The compression performance of Advanced Pore Morphology (APM) foam-filled tubes was evaluated in Ref. [12], where it was demonstrated that polyamide-bonded APM foam-filled tubes are equivalent to traditional foam-filled tubes, demonstrating a similar compressive stress-strain relationship. However, as compared to traditional foam-filled tubes, the Specific Energy Absorption (SEA) is greater in the case of polyamide-bonded APM foam-filled tubes. The addition of silicon filler to the open-cell foam core can further enhance the performance, resulting in a polymer-aluminium alloy hybrid foam that may be utilised as a core for foam-filled tubes [13]. In comparison to empty tubes, hybrid foam-filled structures showed an increase in specific energy absorption of up to 78%. In addition, the shape of the core might be tailored to the exact load, as presented in Ref. [14], where the aluminium tubes filled with bioinspired cores of closed-cell aluminium foam were studied. The results revealed that nine of the twelve bionic samples had a higher energy absorption capacity than the fully-filled samples. The introduction of auxeticity (negative Poisson's ratio) to the core material shows that the auxetic foam-filled square tube is superior to empty and conventional foam-filled square tubes in terms of all evaluated crashworthiness indicators [15,16]. Different spatial distributions of foam filler in tubes were studied by Li et al. [17]. Their findings revealed that the foam-filled double circular tube with the most stable fracture behaviour promises the best energy absorption design. The single and multi tubes approach was also studied, where the multi-tube designs were found to be energetically more effective than single ones at similar foam-filler densities, proving a higher interaction effect [18].

The results of all the above studies show that reinforcing foams contribute to a higher energy absorption capacity of the structure. Research in the field of foam-filled tubes shows a clear trend that the interaction effect benefits the energy absorption capabilities and reduces the force peak. However, the interaction effect can be even larger if the density of the foam is optimised to the specific application needs and the tube stiffness [19]. As a result, foam-filled tubes are among the most promising possibilities for future crash-absorbing components in the fields of crashworthiness, blast, and impact protection. This is due to its lightweight design, enormous capacity of energy absorption, and adoption capabilities. In recent years, additive manufacturing has allowed researchers to precisely design the geometry of cellular structures and create extremely complex shapes like TPMS cellular structures [20]. Surface-based TPMS cellular structures provide superior mechanical properties compared to strut-based cellular structures and, therefore make them great candidates for advanced foam-filled tubes, i.e. TPMS-filled tubes. This was already presented in the recent work of Yin et al. [21], where they studied axial compression behaviour of ex-situ TPMS-filled tubes filled with different TPMS geometries. The interaction between the foam and tube increases the energy absorption capabilities. Nevertheless, using the in-situ TPMS-filled tubes, this effect could be even more pronounced.

Therefore, it is crucial to study also the mechanical behaviour of in-situ TPMS-filled tubes under different loading directions to provide the guidelines for future real-life applications of these modern composites. In this work, the additively manufactured TPMS core, empty tubes, in-situ TPMS-filled tubes, and as-fabricated welded tubes (for assembling the ex-situ TPMS-filled tubes) were tested under compression loading in the axial and transversal direction. The experimental data were used to validate the developed homogenised computational model, which allows the study of the large-scale crash and impact scenarios of real-life applications.

2. Methods

2.1. Geometry and fabrication of specimens

Five different groups of samples were considered in this work. Three have been fully additively manufactured, namely, the lattice cores, empty tubes, and in-situ TPMS-filled tubes (Fig. 1). The other two groups include as-fabricated tubes and hybrid samples. The hybrid samples (ex-situ TPMS-filled as-fabricated tubes) comprise the lattice cores and as-fabricated tubes. They were produced by inserting the lattice core in the as-fabricated tube to create the ex-situ TPMS-filled tubes. The lattices were designed and generated using the MSLattice [22]. The diamond unit cell was chosen for the analysis due to its superior mechanical properties [23]. Lattices were designed with 10% relative density and 5 mm unit cell size. Samples were designed with dimensions 20 (18) mm × 20 (18) mm × 20 mm in the case of short samples and 20 (18) mm × 20 (18) mm × 40 mm for long samples (dimensions given in brackets define the core dimensions), given in the *transversal* × *transversal* × *axial direction* (Fig. 1). For each group of samples, six specimens were fabricated.

The additively manufactured samples were fabricated using the powder bed fusion system EOS M280. This additive manufacturing machine uses a 400 W Ytterbium fibre laser with a beam diameter between 100 μm and 500 μm, and scan speeds up to 7 m/s. The EOS standard printing parameters were used where the build platform was heated to 80 C, the build chamber was purged with Argon gas to prevent oxidation, the layer thickness was set to 20 μm, the hatching spacing was 90 μm the scan speed was variable up to 7 m/s, the hatching scan was rotated 90° after each layer. Gas atomised stainless steel 316L powder was used to fabricate the samples with consistent and repeatable geometry [23]. The used powder was a mix of 50% fresh powder and 50% reused powder. Fig. 2a shows an SEM image of the powder. A clear distinction can be made between the fresh powder, which exhibits a semi-spherical morphology and the reused powder, which departs from the spherical shape. Fig. 2b shows a histogram of the powder size distribution, which indicates an average particle size of 28 μm in diameter and a standard deviation of 16 μm. On the other hand, the as-fabricated tubes were made using the high-frequency induction welding from 304-grade stainless steel provided by Marchegaglia company and cut to the dimension of the sample using a CNC saw. While the two alloys vary significantly in their corrosion resistance, both have tensile and yield properties within 10% difference which was considered an acceptable range of tolerances in this work.

2.2. Experimental testing

The dimensions of the samples were measured with a digital calliper, while the weight was evaluated using the laboratory scale with 0.01 g sensitivity. The experimental tests were performed using the electromechanic loading machine Instron 3382 (Instron, USA) with a 100 kN load capacity. The quasi-static uni-axial compression experiments were carried out as displacement driven with a constant loading rate set to 80 μm/s corresponding to strain-rate of 0.004 s^{-1} and 0.002 s^{-1} for short

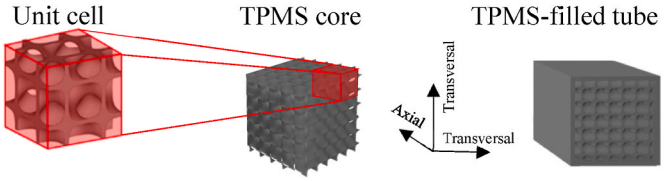

Fig. 1. Computer-aided design models of the short sheet-based TPMS lattices with defined axial and transversal loading directions.

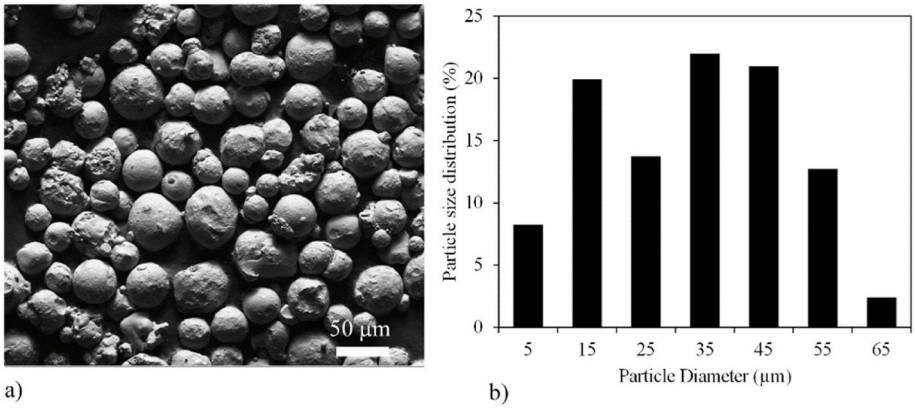

Fig. 2. a) Gaz atomised stainless steel powder, and b) histogram of the particle size distribution of the used powder.

and long samples respectively. The test limit was set for all samples to the strain of 0.8 or force of 90 kN. The plateau stress was calculated as average stress in the range of 20–40% compressive strain [24], while the Specific Energy Absorption (SEA) was calculated with the integration of compression response up to 40% strain and divided by the density of samples. The mechanical responses in Figs. 7, 9 and 11 are shown with standard deviation, while the sum of the responses of empty tubes and core are also presented to evaluate the interaction effect in the case of TPMS-filled tubes. The sum is calculated as as-fabricated tube and core in the case of ex-situ TPMS-filled tubes and additively manufactured tube and core in the case of in-situ TPMS-filled tubes.

For full-field displacement and strain evaluation, the experiments were observed optically using bi-telecentric zoom lens TCZR072 (Opto Engineering, Italy) mounted on monochromatic camera Manta G-504B (AVT, Germany) with the resolution of 2452 px × 2056 px. The loading scene was uniformly illuminated by pair of cold-light LED bars LTBRDC series (Opto Engineering, Italy). The image data was acquired with a frequency of 2 Hz. The applied force and cross-head displacement were sampled at a 10 Hz frequency. Full-field displacement and strain evaluation was performed using an in-house developed Python algorithm employing the Digital Image Correlation (DIC) technique. This method combines image registration and tracking to identify changes in a sequence of images. The DIC tool achieves subpixel tracking precision. First, the correlation is evaluated on a pixel level employing the template matching technique with the use of the Sum of Squared Differences (SSD) method given as:

$$R(x,y) = \sum_{x',y'} (T(x',y') - I(x+x',y+y'))^2, \quad (1)$$

where R is the template matching result matrix, T is the template image (subset) and I represents the source image (offset). Then the pixel level correlation values are interpolated by a third-order bivariate spline and then minimised to obtain the best match on the subpixel level using the Limited-memory Broyden-Fletcher-Goldfarb-Shanno optimisation algorithm [25]. The strain field of the specimen is obtained by processing the displacement field. The displacement of the correlation points represents the displacement of nodes in terms of finite elements, therefore assuming a rectangular grid of correlation points, the strain field can be observed by employing a mesh of planar quadrilateral elements. To compare the experimental and numerical results, the principal strain was used. Experimental results are represented by the coloured principal strain fields mapped on corresponding image data (Fig. 3).

2.3. Computational modelling

The computational models of TPMS lattices were generated using the shell finite elements (FE) using the MSLattice code to generate the mid-surface lattice geometry of TMPS samples [22]. Spatial discretisation was performed by the PrePoMax software [26], and the boundary conditions were defined in the LS-PrePost software. The simple homogenised material model was used for modelling the TPMS samples, which offers the fast and accurate prediction of cellular structure's behaviour and can be used in large-scale structural integrity simulations, e.g. impact, crash. The explicit solver of the LS-DYNA finite element software system [27] was used for all presented computer simulations.

2.3.1. Material model

The elastoplastic material model (MAT_024) was used to describe the base material constitutive relation of the analysed tubes, while the homogenised crushable foam material model (MAT_063) was applied for TPMS lattices [27]. TPMS lattices were modelled with the solid finite elements in contrast to the detailed geometry used in Ref. [28], which offer a straightforward and fast calculation of the global cellular structure's deformation, while it is not possible to observe in detail the deformation process of the detailed cellular structure. The hardening behaviour of the material model was defined according to the results of quasi-static uniaxial compression testing [29]. Inverse computational simulations of loaded empty and filled tubes were performed to retrieve the same macroscopic simulation results as those measured in experimental testing for all analysed geometries up to densification. The material parameters of the material model MAT_024 are given in Table 1. The values of yield stresses for AISI 361L additively fabricated tubes are

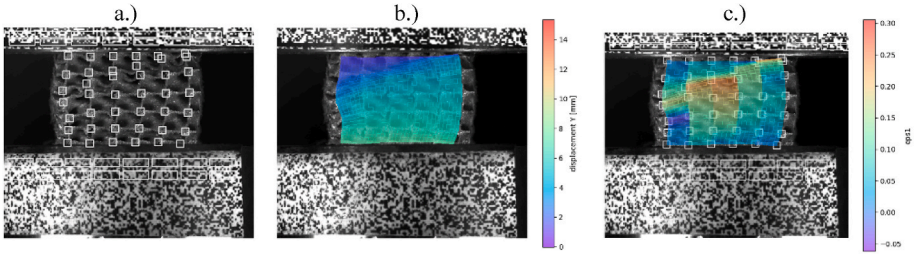

Fig. 3. The DIC procedure: a.) correlation points, b.) vertical displacements, and c.) principal strains.

Table 1
The MAT_024 material model parameters.

Sample	ρ [kg/m^3]	E [GPa]	ν [−]	σ_{yield} [MPa]	σ_2 [MPa]	$\varepsilon_{pl,2}$ [−]
As-fabricated tube	7850	210	0.3	284	624	0.56
Additively fabricated tube				450	650	0.30

The top and bottom compression plates were modelled as linear-elastic (material model MAT_ELASTIC) with the following material parameters: density $\rho = 7850$ kg/m^3, Young's modulus $E = 210$ GPa and the Poisson's ratio $\nu = 0.3$.

similar to those reported in Ref. [30], where the material parameters were determined using different standard tensile and shear specimens. The material parameters for the as-fabricated tubes were given by the tube's certificate provided by Marchegaglia company (yield stress: 284 MPa, tensile strength: 624 MPa, and strain at fracture: 50.6%). The parameters for the material model are following: density ρ, Young's modulus E, Poisson's ratio ν, initial yield stress σ_{yield}, linear hardening model with the second point in the stress-strain diagram (σ_2, $\varepsilon_{pl,2}$). Ideal plasticity was assumed after the $\varepsilon_{pl,2}$ to avoid non-physical removal of FE in the case of considered failure.

2.3.2. Boundary conditions and finite element mesh

A fully integrated shell FE with two through-thickness integration points was used to discretise the tube's geometry, while the fully integrated solid FE was used for the homogenised core. The mesh sensitivity analysis was performed with three different FE meshes and three different numbers of through-thickness integration points. The approximate global size of FE was 0.25 mm, which results in approx. 640 elements for the tube, 810 elements for the homogenised core. The Belytschko-Tsay shell FE with two through-thickness integration points and a thickness of 1 mm was used to model the compression plates [27].

The following boundary conditions were used: the bottom support with all degrees of freedom fixed, the top support with a prescribed constant velocity of 2 m/s in the z-axis direction (Fig. 4). The increase in quasi-static testing velocity was used to speed up the simulations and was confirmed as acceptable by parametric computational analysis, where the reaction forces on the bottom and upper plate were compared at different loading velocities to study the inertia effect of the sample's mass.

The node to surface contact formulation with friction (static and dynamic friction coefficients were set to 0.36 and 0.34, respectively [31]) was defined between tube and supports. The node to surface tied contact with the tiebreak option was used for the contact between the tube and core in case of in-situ TPMS-filled tubes.

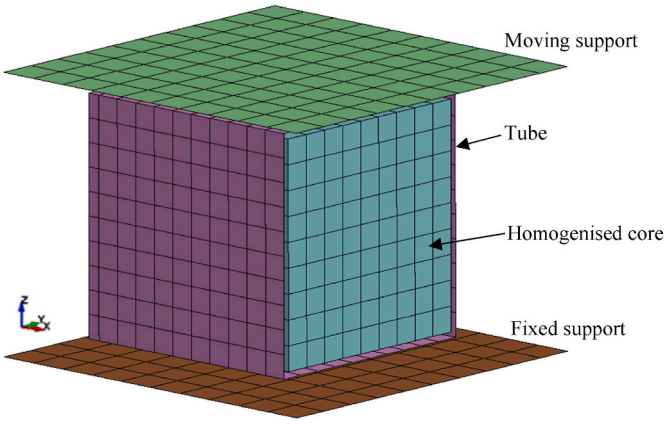

Fig. 4. Computational model of TPMS-filled tube positioned in the transversal loading direction.

3. Geometrical characterisation

Fig. 5a shows images of the five different samples considered in this work. The Additively manufactured samples were blasted with high-pressure air to remove the residual powder and were then weighted and the actual dimensions were measured. The wall thickness of the additively-manufactured tube was 0.98 mm while the wall thickness of as-fabricated tubes was 0.94 mm. This is the reason for the difference in weight between the two types of empty tubes. The weights of fabricated samples are given in Table 2.

The scanning electron microscopy images in Fig. 5bI-IV provide information about the geometrical features of the manufactured samples. For example, Fig. 5I shows a section of the additively manufactured tube. The hatching and contour tracks are visible. Also, surface roughness due to powder adhesion to the walls can be observed. Fig. 5II shows a top view of the fabricated Diamond lattice core. The figure shows well-defined cells with no obvious micro-cracks or micro-voids despite the low relative density of 10%. Fig. 5III shows an SEM image of the foam-filled tube and Fig. 5IV zooms into the structure of Fig. 5III to show the seamless transition between the boundary of the tube and the diamond lattice core.

4. Experimental testing results

4.1. Axial loading

The experimental results of axial loading of short samples are shown in Figs. 6 and 7. The deformation behaviour of all five analysed sample groups in the axial direction is given with DIC plots of principal strains in Fig. 6. The deformation of the core is initially mostly formed in a shear plane under 45° at displacements up to 10 mm and then localised in the middle of the sample at higher displacements (Fig. 6a). The deformation of empty tubes is different since, in the case of the as-fabricated tube, the lobes are formed inwards, which can be a consequence of the tube's fabrication procedure (welding), while the lobes are formed outwards in the case of additively manufactured tubes. The TPMS-filled tubes showed similar deformation behaviour with the localisation of the deformation in the middle of the height of the samples. The lobes are much more localised in the case of in-situ TPMS-filled tubes, which means that in the localised part the tube-core connection fails, and the lobe can be formed there. In the case of ex-situ TPMS-filled tubes, the tube did not deform inwards, like in the case of an empty tube, which caused the lobes to form outward like in the case of in-situ TPMS-filled tubes.

The mechanical responses presented in Fig. 7 show a long flat plateau section of TPMS core samples and degressive mechanical response of as-fabricated tubes (as-fab tube) and additively manufactured tubes (3D print tube) after the initial force peak. The as-fabricated tubes show higher initial force peaks compared to additively manufactured tubes, which is a consequence of the better ductility of the as-fabricated tubes (Table 1), while the overall energy absorption capabilities are comparable with additively manufactured tubes, which are analysed in detail in section 4.3. The mechanical response of ex-situ TPMS-filled tubes and in-situ TPMS-filled tubes provide a much higher mechanical response than empty tubes or cores and offer better energy absorption capabilities. The enhancement of the mechanical response is presented in Fig. 7 with the shaded area, representing the interaction effect in the case of in-situ TPMS-filled tubes. The enhancement is better in the case of in-situ TPMS-filled tubes due to the connection between the tube's inner surface and the core, where it can be observed that the deformation behaviour is changed (Fig. 6) in that way, that the lobes of the foam-filled tube are formed later in the case of the in-situ TPMS-filled tubes. Also, the stiffness combination of the core and tube should be considered, as the stiffness of the additively manufactured tube is a bit lower than the as-fabricated tube. This can contribute to a more uniform stress distribution between the core and tube in the case of in-situ TPMS-filled

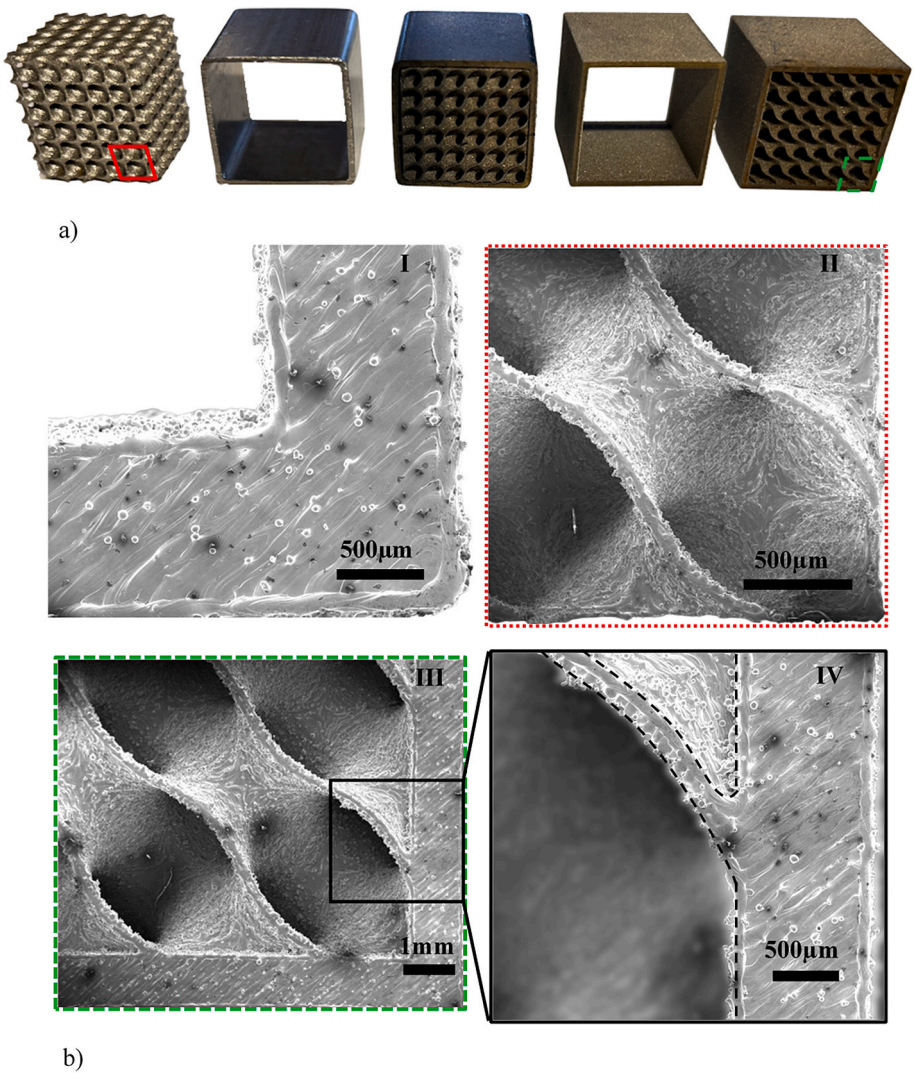

Fig. 5. a) Images of the five different samples considered in this work from left to right: lattice core, commercial tube, ex-situ foam filled tube, additively manufactured tube, and in-situ foam filled tube. b) SEM images showing the geometrical features of the fabricated sample.

Table 2
Weight of the samples (st. deviations are shown in brackets).

Weight (st.dev) [g]					
Sample	Core	As-fabricated tube	3D printed tube	Ex-situ TPMS-filled tube	In-situ TPMS-filled tube
Short	7.67 (0.05)	11.20 (0.08)	11.64 (0.03)	18.83 (0.17)	19.48 (0.10)
Long	15.46 (0.07)	22.76 (0.10)	23.37 (0.06)	37.95 (0.20)	39.37 (0.15)

tubes and also reflects on the global mechanical response.

The experimental results of axial loading of long samples are given in Figs. 8 and 9. The deformation behaviour of the cores, additively manufactured tubes, and in-situ TPMS-filled samples are shown in Fig. 8. Since the mechanical properties of these samples differ the most from the results of short samples (Fig. 12), their deformation behaviour was analysed in detail. The core (Fig. 8a) fails similar to the case of short samples (Fig. 6a), where the shear plane is formed. The shear plane is formed under an identical angle in both cases. Therefore, the failure is localised in the middle of the long sample, where the slip happens after failure at approx. 12 mm displacement and the deformation continue up to the densification in two separate parts of the sample. Due to this reason, the plateau and SEA values are much lower in the case of long samples.

The additively manufactured tube deformation behaviour is much more unstable in the case of long samples (Fig. 8b) than in the case of short samples (Fig. 6c), which is also reflected in the mechanical response discrepancy (Fig. 9). The plateau stress and SEA are in most cases decreased in the case of long additively manufactured tubes. However, a much larger standard deviation should also be considered, especially in the case of plateau stress (Fig. 12).

The deformation behaviour of the in-situ TPMS-filled tubes (Fig. 8c) is very similar to the ones observed in the case of short samples (Fig. 6e). The only difference is that two lobes are formed in the case of long samples.

The mechanical responses of long samples in the axial loading direction are given in Fig. 9, where the relationship between the groups of the samples is very similar to the ones already discussed for the short samples. The enhancement of the mechanical responses in the case of long TPMS-filled tubes is also presented and evident in Fig. 9. The shaded area represents the interaction effect in the case of in-situ TPMS-filled tubes. The discrepancy between the short and long samples loaded in the axial direction is provided in Section 4.3.

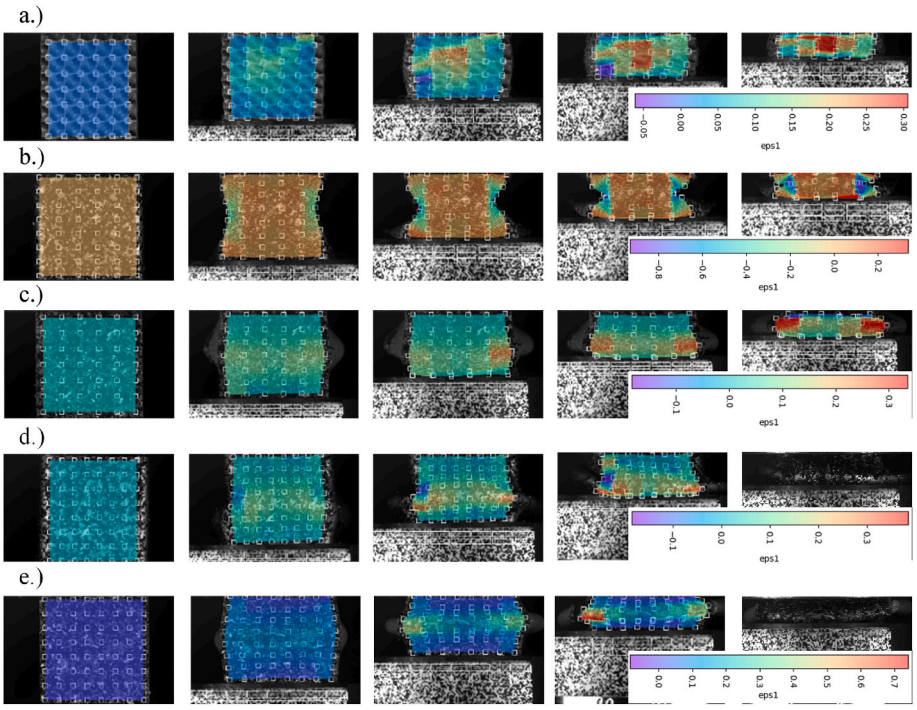

Fig. 6. Deformation behaviour of short samples in axial direction: a.) lattice core, b.) as-fabricated tube, c.) additively manufactured tube, d.) ex-situ TPMS-filled tubes and e.) in-situ TPMS-filled tubes (displacement increment 4 mm).

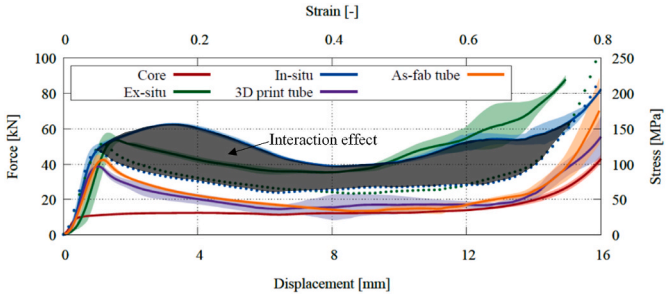

Fig. 7. Mechanical response of short samples in axial direction with illustrated interaction effect for in-situ TPMS-filled structures (the sum of the empty tubes and core is given by dotted curves).

4.2. Transversal loading

The experimental results of transversal loading of short samples are given in Figs. 10 and 11. The core's deformation pattern (Fig. 10a) is very similar to one observed in the case of axial loading (Fig. 6a). While the deformation pattern of the core is not changed in the case of transversal loading, the deformation pattern of empty tubes changes significantly. As expected, the two sides of empty tubes (oriented in the loading direction) buckle outwards (Fig. 10b and c). The same also happens in the case of ex-situ TPMS-filled tubes (Fig. 10d), where there is no connection between the core and tubes. The connection between the tube and core in the case of in-situ TPMS-filled tubes remains up to the densification of the samples and is therefore capable of preventing the tube from buckling outwards and detaching from the core (Fig. 10e).

The mechanical responses of samples loaded in the transversal direction are given in Fig. 11. It can be observed that the empty tubes provide a much less stiff response than in the case of axial direction due to the buckling of the tube's walls. Therefore, also the ex-situ TPMS-filled tubes provide only a slightly stiffer response than the core since the core and the tube are deforming as separate constituents (Fig. 10d). The connection between the core and tube in the case of in-situ TPMS-filled tubes enables the interaction effect of tube and core also in the case of transversal loading. The interaction effect is presented in Fig. 11 with the shaded area.

4.3. Results analysis

The values of plateau stress and SEA for all analysed samples (loaded in axial and transversal directions) are given in Fig. 12, where also the standard deviations are plotted with error bars. In the case of cores, it is evident that the core is stiffer in the transversal direction, while the longer core is less stiff than the short one. This is a consequence of the changed deformation mode, as discussed in Section 4.1. Despite cubic symmetry, the properties of the lattice cores in the transverse and axial directions are slightly different. This difference is largely influenced by the internal density of cracks and micro-voids in the bulk of the TPMS diamond sheets, especially at such a low relative density and small cell size.

In the case of the empty tubes, the responses of short and long samples are comparable for the axial loading direction, while in general as-fabricated tubes provide higher plateau stresses and SEA. In the case of transversal loading, the stiffness of empty tubes is drastically decreased due to the buckling of tube walls.

The interaction effect in the case of TPMS-filled tubes is marked with chequered area in Fig. 12b, where the SEA values of in-/ex-situ TPMS-filled tubes are compared to the highest SEA from the core and empty tubes. As it can be observed, the greatest SEA improvement is achieved in the case of in-situ TPMS-filled tubes in axial (37% improvement in case of short and 44% improvement in case of long samples) and transversal loading direction (12% improvement). In the case of ex-situ TPMS-filled tubes, the SEA enhancement is lower and limited to the axial loading. However, the SEA improvement is still 21% in the case of short samples and 18% in the case of long samples.

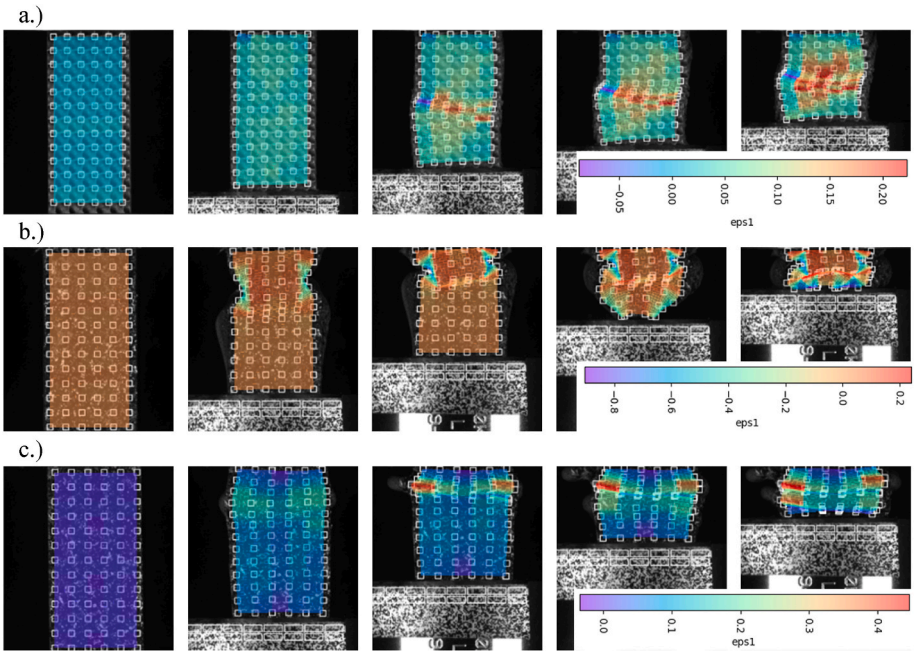

Fig. 8. Deformation behaviour of long samples in axial direction: a.) lattice core, b.) additively manufactured tube, and d.) in-situ TPMS-filled tubes (displacement increment 6 mm).

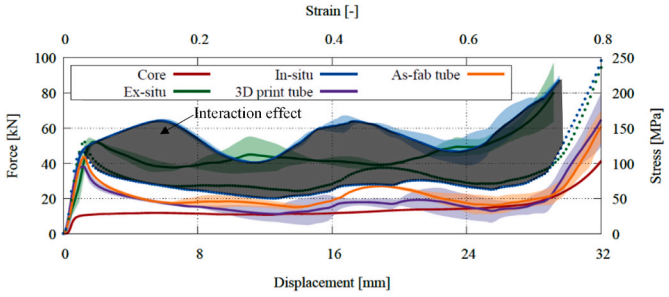

Fig. 9. Mechanical response of long samples in the axial direction with illustrated interaction effect for in-situ TPMS-filled structures (the sum of the empty tubes and core is given by dotted curves).

5. Computational simulations

5.1. Validation of the computational model

The computational models were validated only for the short samples since the computational models of long samples can be easily adapted later. They were loaded in axial and transversal directions. The comparison between the results of the computational model and experiments is shown in Fig. 13. The computational results of core in both loading directions are basically identical to the experimental ones since the experimental results were used for the definition of the homogenised computational model. In the case of axial loading, the first force peak is underestimated in the case of as-fabricated tubes, while the response is stiffer at larger strains. The computational model of additively manufactured tubes captures the behaviour from the experiments much better. In the case of transversal loading, the mechanical response of tubes is very similar to the experimental observations up to a strain of 50%, after which, the response of the computational model is slightly stiffer, due to the out-of-plane bending of shell finite elements.

The computational models of TPMS-filled tubes capture the overall experimental response well in the wide range of strains (up to the densification) in the case of transversal loading. A larger discrepancy can be observed in the case of axial loading, in which a more non-linear response with several contacts is causing instabilities in the computational response. Overall, the comparison between the experimental and the computational results is in good agreement from the view of plateau stress and SEA, which are the most important properties in the case of impact and crash protection. In the case of axial loading, the computational SEA is 3% overestimated for ex-situ TPMS-filled tubes and 2% estimated for in-situ TPMS-filled tubes compared to the experimental values. The computational plateau is 13% overestimated for ex-situ TPMS-filled tubes and 1% estimated for in-situ TPMS-filled tubes.

In the case of transversal loading, the SEA is 1% overestimated for ex-situ TPMS-filled tubes and 4% estimated for in-situ TPMS-filled tubes. The plateau is also in good correlation (2% overestimated) in the case of ex-situ TPMS-filled tubes. However, a 14% overestimation was noted in the case of in-situ TPMS-filled tubes.

The deformation behaviour of the computational model is accurately capturing the experimental behaviour. At this point, it should be noted that in the case of in-situ TPMS-filled tubes, the nodes of the core are moved to the surface of the tube to assure the tied connection. This does not affect the global mechanical response but reflects only in the visualisation, which can be observed in Figs. 14 and 15. The ex-situ and in-situ TPMS-filled tubes deformation behaviour under axial loading are shown in Fig. 14, where it can be observed that the experimental deformation mode of the analysed samples (Fig. 6d and e) is captured correctly with the computational model. The larger difference in the deformation behaviour between the ex-situ and in-situ TPMS-filled tubes is observed in the case of transversal loading (Fig. 15). It is also in perfect analogy with the experimental results Fig. 10d and e. The buckling of the tube in the case of ex-situ TPMS-filled tubes is captured with the computational model very precisely (Fig. 15b).

6. Conclusions

The ex-situ and in-situ TPMS-filled tubes were fabricated and compressively tested in axial and transversal loading directions. Besides TPMS-filled tubes also its constituents were tested, i.e. empty tubes and TPMS core. The experimental testing reveals good repeatability in all analysed loading cases and geometries. The following conclusions can be drawn from the experimental tests:

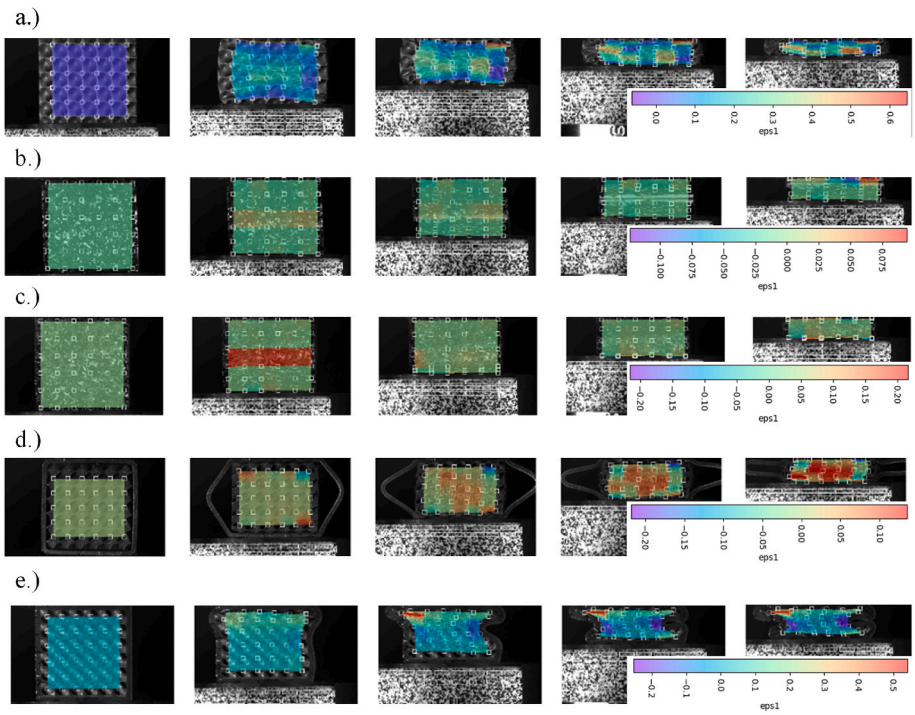

Fig. 10. Deformation behaviour of short samples in the transversal direction: a.) lattice core, b.) as-fabricated tube, c.) additively manufactured tube, d.) ex-situ TPMS-filled tubes, and e.) in-situ TPMS-filled tubes (displacement increment 4 mm).

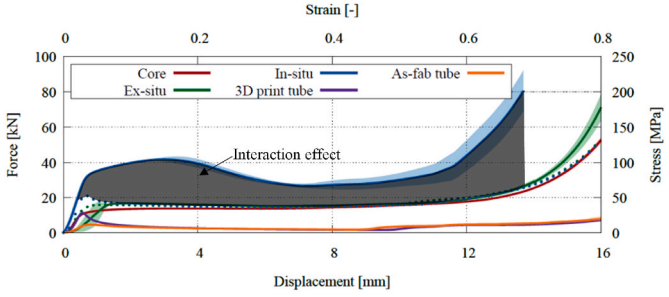

Fig. 11. Mechanical response of short samples in the transversal direction with illustrated interaction effect for in-situ TPMS-filled structures (the sum of the empty tubes and core is given by dotted curves).

- The length of the samples in the case of axial loading changes the deformation behaviour mainly in the case of core, additively fabricated tubes, and in-situ TPMS-filled tubes. This is mostly connected to the localisation of the deformation;
- The testing in axial and transversal loading directions showed that the energy absorption capabilities are much higher in the case of axial loading due to the buckling of the tube walls in the case of transversal loading. This was successfully avoided in the in-situ TPMS-filled tubes, where the connection between the tube and the core prevents the buckling of the tube's walls;
- The force drop after the initial force peak was successfully eliminated using the TPMS-filled structures, which provide much more stable deformation and mechanical response and better and more reliable energy absorption capabilities;
- In the axial loading direction, the energy absorption is enhanced by up to 44% in the case of in-situ TPMS-filled structures and up to 21% in the case of ex-situ TPMS-filled structures compared to the as-fabricated empty tube, which has the highest SEA of empty tubes and core;
- In the transversal loading direction, the SEA enhancement is observed only in the case of in-situ TPMS-filled tubes, where the SEA is enhanced up to 12%.

The SEA enhancement of TPMS-filled tubes is in general, higher

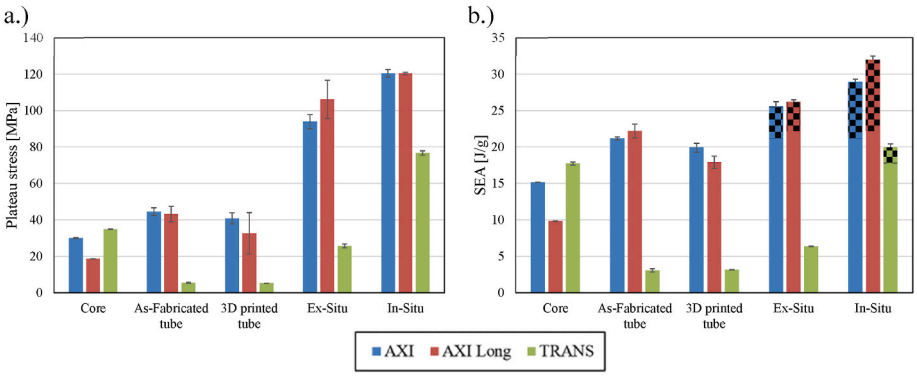

Fig. 12. The plateau stress a.) and SEA b.) analysis of lattice cores, empty tubes and TPMS-filled tubes.

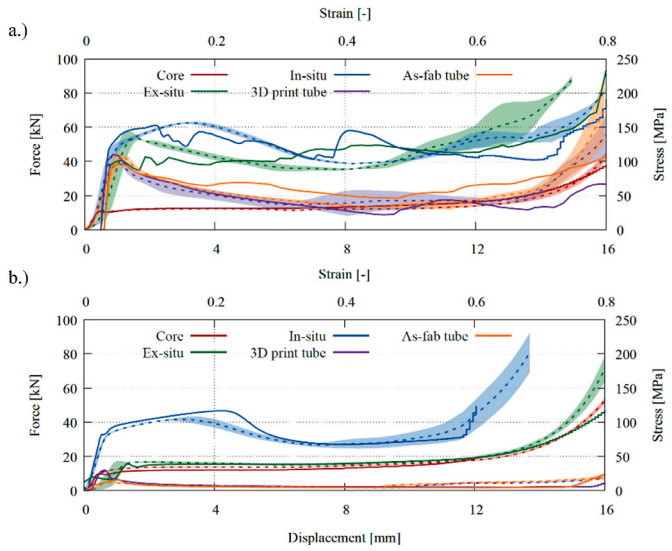

Fig. 13. Comparison between the experimental (dotted lines) and computational (solid lines) results of short samples in axial a.) and b.) transversal direction.

when compared to values presented in previous work for aluminium open-cell foam-filled tubes (1.5% enhancement) [11], APM (Advanced Pore Morphology) foam-filled tubes (7–14% enhancement) [12] and closed-cell foam-filled tubes (13–60% enhancement) [10]. As can be seen from different achieved levels of SEA enhancement, the ratio stiffness of filler and tube plays a crucial role, which can also be controlled by adding the hybrid foams, as shown in Ref. [11].

Based on the experimental data, the computational models were developed and validated. A straightforward homogenised computational model of core was developed to provide the possibility to use the fast and accurate computational model of TPMS-filled tubes in large-scale simulations. The deformation behaviour and the overall energy absorption capabilities were captured well with the computational models of in-situ and ex-situ TPMS-filled tubes, which now offer the framework to extensively study the behaviour of TPMS-filled tubes in real-life applications.

CRediT authorship contribution statement

Nejc Novak: Conceptualization, Investigation, Writing – original draft. **Dan Kytyr:** Investigation, Methodology, Writing – review & editing. **Vaclav Rada:** Investigation, Methodology, Writing – review & editing. **Tomas Doktor:** Investigation, Methodology, Writing – review & editing. **Oraib Al-Ketan:** Conceptualization, Investigation, Methodology, Writing – original draft. **Reza Rowshan:** Conceptualization, Funding acquisition, Resources, Writing – review & editing. **Matej**

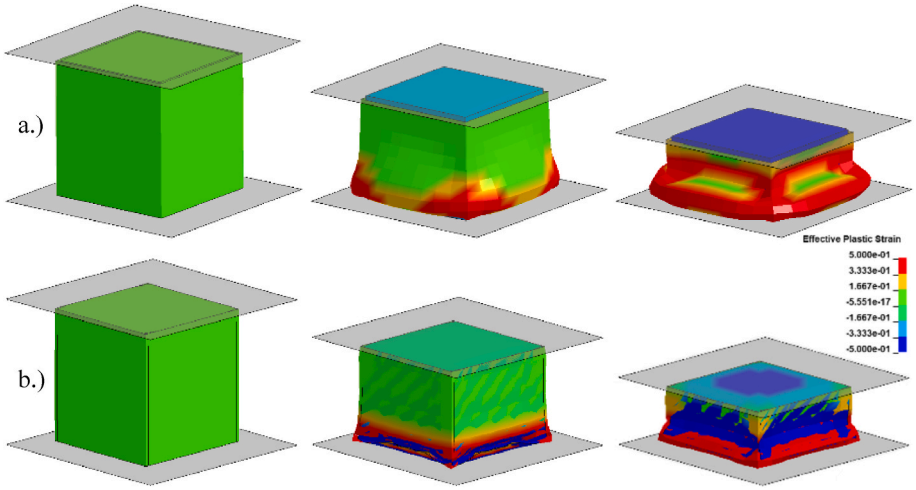

Fig. 14. Deformation behaviour of a computational model of ex-situ a.) and in-situ b.) TPMS-filled tubes in the axial direction (displacement increment 6 mm).

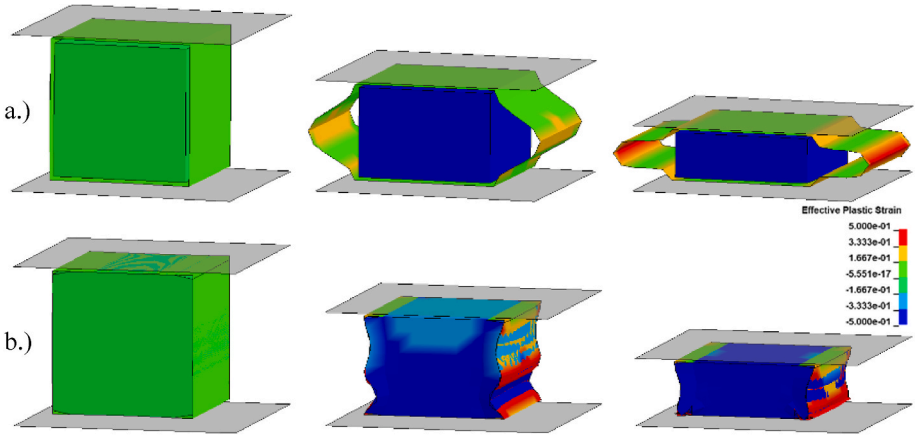

Fig. 15. Deformation behaviour of a computational model of ex-situ a.) and in-situ b.) TPMS-filled tubes in the transversal direction (displacement increment 6 mm).

Vesenjak: Conceptualization, Supervision, Validation, Writing – review & editing. **Zoran Ren:** Conceptualization, Funding acquisition, Supervision, Validation, Writing – review & editing.

Declaration of competing interest

The authors declare that they have no known competing financial interests or personal relationships that could have appeared to influence the work reported in this paper.

Data availability

Data will be made available on request.

Acknowledgments

The authors acknowledge the financial support from the Slovenian Research Agency (fundamental postdoctoral research project (No. Z2-2648) and national research programme funding (No. P2-0063)). This research was partially carried out using the Core Technology Platforms resources at New York University Abu Dhabi and by the Czech Science Foundation (project No. 19-23675S).

References

[1] T. Wierzbicki, W. Abramowicz, On the crushing mechanics of thin-walled structures, J. Appl. Mech. 50 (1983) 727–734, https://doi.org/10.1115/1.3167137.
[2] G.M. Nagel, D.P. Thambiratnam, Dynamic simulation and energy absorption of tapered thin-walled tubes under oblique impact loading, Int. J. Impact Eng. 32 (2006) 1595–1620, https://doi.org/10.1016/J.IJIMPENG.2005.01.002.
[3] S.E. Alkhatib, F. Tarlochan, A. Eyvazian, Collapse behaviour of thin-walled corrugated tapered tubes, Eng. Struct. 150 (2017) 674–692, https://doi.org/10.1016/J.ENGSTRUCT.2017.07.081.
[4] A.A. Nia, J.H. Hamedani, Comparative analysis of energy absorption and deformations of thin walled tubes with various section geometries, Thin-Walled Struct. 48 (2010) 946–954, https://doi.org/10.1016/J.TWS.2010.07.003.
[5] L.J. Gibson, M.F. Ashby, Cellular Solids: Structure and Properties, Cambridge University Press, Cambridge, U.K., 1997.
[6] M.F. Ashby, A. Evans, N.A. Fleck, L.J. Gibson, J.W. Hutchinson, H.N.G. Wadley, Metal Foams: a Design Guide, Elsevier Science, Burlington, MA, Massachusetts, 2000, https://doi.org/10.1016/S0261-3069(01)00049-8.
[7] D. Lehmhus, M. Vesenjak, S. de Schampheleire, T. Fiedler, From stochastic foam to designed structure: balancing cost and performance of cellular metals, Materials 10 (2017) 1–32, https://doi.org/10.3390/ma10080922.
[8] M. Vesenjak, T. Fiedler, Z. Ren, A. Öchsner, Behaviour of syntactic and partial hollow sphere structures under dynamic loading, Adv. Eng. Mater. 10 (2008) 185–191, https://doi.org/10.1002/adem.200700325.
[9] A.G. Hanssen, M. Langseth, O.S. Hopperstad, Static and dynamic crushing of square aluminum extrusions with aluminum foam filler, Int. J. Impact Eng. 24 (2000) 347–383, https://doi.org/10.1016/S0734-743X(99)00169-4.
[10] I. Duarte, L. Krstulović-Opara, M. Vesenjak, Characterisation of aluminium alloy tubes filled with aluminium alloy integral-skin foam under axial compressive loads, Compos. Struct. 121 (2015) 154–162, https://doi.org/10.1016/j.compstruct.2014.11.003.
[11] I. Duarte, M. Vesenjak, L. Krstulović-Opara, Z. Ren, Static and dynamic axial crush performance of in-situ foam-filled tubes, Compos. Struct. 124 (2015) 128–139, https://doi.org/10.1016/j.compstruct.2015.01.014.
[12] I. Duarte, M. Vesenjak, L. Krstulović-Opara, Z. Ren, Compressive performance evaluation of APM (Advanced Pore Morphology) foam filled tubes, Compos. Struct. 134 (2015) 409–420, https://doi.org/10.1016/j.compstruct.2015.08.097.
[13] I. Duarte, L. Krstulović-Opara, J. Dias-de-Oliveira, M. Vesenjak, Axial crush performance of polymer-aluminium alloy hybrid foam filled tubes, Thin-Walled Struct. 138 (2019) 124–136, https://doi.org/10.1016/j.tws.2019.01.040.
[14] J. Song, S. Xu, L. Xu, J. Zhou, M. Zou, Experimental study on the crashworthiness of bio-inspired aluminum foam-filled tubes under axial compression loading, Thin-Walled Struct. 155 (2020), 106937, https://doi.org/10.1016/j.tws.2020.106937.
[15] S. Mohsenizadeh, R. Alipour, M. Shokri Rad, A. Farokhi Nejad, Z. Ahmad, Crashworthiness assessment of auxetic foam-filled tube under quasi-static axial loading, Mater. Des. 88 (2015) 258–268, https://doi.org/10.1016/j.matdes.2015.08.152.
[16] S. Mohsenizadeh, Z. Ahmad, Auxeticity effect on crushing characteristics of auxetic foam-filled square tubes under axial loading, Thin-Walled Struct. 145 (2019), 106379, https://doi.org/10.1016/j.tws.2019.106379.
[17] Z. Li, R. Chen, F. Lu, Comparative analysis of crashworthiness of empty and foam-filled thin-walled tubes, Thin-Walled Struct. 124 (2018) 343–349, https://doi.org/10.1016/J.TWS.2017.12.017.
[18] M. Güden, H. Kavi, Quasi-static axial compression behaviour of constraint hexagonal and square-packed empty and aluminum foam-filled aluminum multi-tubes, Thin-Walled Struct. 44 (2006) 739–750, https://doi.org/10.1016/J.TWS.2006.07.003.
[19] H.R. Zarei, M. Kröger, Optimisation of the foam-filled aluminum tubes for crush box application, Thin-Walled Struct. 46 (2008) 214–221, https://doi.org/10.1016/J.TWS.2007.07.016.
[20] O. Al-Ketan, R. Rowshan, R.K.R. Abu Al-Rub, Topology-mechanical property relationship of 3D printed strut, skeletal, and sheet based periodic metallic cellular materials, Addit. Manuf. 19 (2018) 167–183, https://doi.org/10.1016/j.addma.2017.12.006.
[21] H. Yin, D. Tan, G. Wen, W. Tian, Q. Wu, Crashworthiness analysis and optimisation design of TPMS-filled structure, Int. J. Crashworthiness (2021) 1–18, https://doi.org/10.1080/13588265.2021.1959171, 0.
[22] O. Al-Ketan, R.K. Abu Al-Rub, MSLattice: A free software for generating uniform and graded lattices based on triply periodic minimal surfaces, Mater. Des. Process. Commun. 3 (2021) 1–10, https://doi.org/10.1002/mdp2.205.
[23] N. Novak, O. Al-Ketan, L. Krstulović-Opara, R. Rowshan, R.K. Abu Al-Rub, M. Vesenjak, Z. Ren, Quasi-static and dynamic compressive behaviour of sheet TPMS cellular structures, Compos. Struct. 266 (2021) 1–10, https://doi.org/10.1016/j.compstruct.2021.113801.
[24] ISO 13314:2011, - Mechanical Testing of Metals - Ductility Testing - Compression Test for Porous and Cellular Metals, International Organization for Standardization, Geneva, Switzerland, 2011. www.iso.org.
[25] D.C. Liu, J. Nocedal, On the limited memory BFGS method for large scale optimisation, Math. Program. 45 (1989) 503–528, https://doi.org/10.1007/BF01589116.
[26] M. Borovinšek, PrePoMax (n.d.), https://prepomax.fs.um.si/.
[27] J. Hallquist, LS-DYNA Keyword User's Manual, Livermore Software Technology Corporation, Livermore, California, 2007.
[28] N. Novak, O. Al-Ketan, M. Borovinšek, L. Krstulović-Opara, R. Rowshan, M. Vesenjak, Z. Ren, Development of novel hybrid TPMS cellular lattices and their mechanical characterisation, J. Mater. Res. Technol. 15 (2021) 1318–1329, https://doi.org/10.1016/j.jmrt.2021.08.092.
[29] N. Novak, M. Vesenjak, Z. Ren, Crush behaviour of auxetic cellular structures, Sci. Technol. Mater. 30 (2018) 4–7, https://doi.org/10.1016/j.stmat.2017.12.003.
[30] X. Li, C.C. Roth, T. Tancogne-dejean, D. Mohr, Rate- and temperature-dependent plasticity of additively manufactured stainless steel 316L: characterisation, modeling and application to crushing of shell-lattices, Int. J. Impact Eng. (2020), 103671, https://doi.org/10.1016/j.ijimpeng.2020.103671.
[31] P.J. Blau, Friction Science and Technology, CRC Press, 2008, https://doi.org/10.1201/9781420054101.